Supporting Information

Grinsted et al. 10.1073/pnas.1209542109

SI Methods

S1. Construction of the Surge Index. The selection criteria for the six tide gauges used in the construction of the surge index are presented in the main text. Here we summarize the steps involved in our calculation of the surge index.

i) For each station we do the following:
  a) Apply a 24-h smoothing to the hourly series, thus obtaining a moving average daily average sea-level series. Gaps shorter than 3 h are in-filled by linear interpolation.
  b) Calculate the squared day-to-day differences from this daily sea-level series.
  c) Down-sample this series to a daily surge series, using daily block maxima.
  d) Remove the annual cycle by division. The different tide-gauge locations have different sensitivities, due to local effects such as bathymetry, and normalizing by the seasonal cycle brings the records to a common reference. The background seasonal cycle is determined from the second percentile of data within a moving 21-d-wide seasonal slice. The estimated seasonal cycle is smoothed using a 180-d-long robust loess filter with periodic boundary conditions.
  e) Decluster the record. Single storm events may cause broad peaks that last several days. We therefore remove samples that are smaller than the local 3-d maximum value.

ii) Combine the six deseasonalized surge records into a single record of daily maximum values. We allow a maximum of one station missing when calculating the maximum value. Declustering (step *i*, *e*) is ignored on the rare dates, when it would have removed data from all six stations.

iii) Rescale the final surge index containing the record of daily maximal surge values to have median = 1.

The conclusions of this paper are insensitive to minor changes in the procedure. However, the justification for our further analysis using the generalized extreme value distribution hinges on the series being approximately stationary on subannual scales. Therefore, the performance of step *i*, *d* is important. We have therefore verified that step *i*, *d* removes the kink in the distribution at frequencies corresponding to annual return periods.

Steps *i*, *a* and *i*, *b* act to remove the tidal signal and the trend. The remaining signal is completely dominated by nontidal components and primarily wind-driven changes in sea level. This can be easily verified as steps *i*, *a* and *i*, *b* can be combined into a simple finite impulse response filter and the resulting frequency response can be examined. As an example, for Mayport the modeled hourly tidal signal [from National Oceanic and Atmospheric Administration (NOAA)] has a SD of 0.50 m; applying step *i*, *a* reduces this to 0.10 m; and applying step *i*, *b* reduces this to 0.01 m. Finally, we have repeated the entire analysis but explicitly remove the tidal signal before step *i*, *a* and obtain near identical results.

There are unfortunately a few gaps in the tide-gauge records, and some of these gaps could have been caused by extreme weather. Here we compare the tide-gauge records with the Atlantic Hurricane Database (HURDAT) to determine which gaps could be caused by the passing of a storm. It is implausible that storms passing close to tide gauges were not well documented. We have chosen a few simple criteria to screen for gaps that might be related to the passing of a storm:

The data gap start must overlap the timing of the storms making landfall within a ±24-h margin.

The storm must have been within 250 km of the tide gauge at the onset of the gap.

The start of the storm must precede the onset of the data gap (allowing for a 6-h slack).

From Table S1 (and Fig. S2) we see that by these criteria only eight data gaps can possibly be related to the passing of a storm. These gaps in the tide-gauge records quite likely correspond to some large storm surges that are missing in the surge index record. We have therefore made a sensitivity test where we set the surge index at the "gap-start" dates manually to have the same magnitude as Hurricane Katrina 2005. Our results are robust to this test.

S2. Events with the Largest Surge Index. In Table S2 we show the surge index of the 50 greatest events. A surge will generally also lead to a secondary peak the following day as sea level returns toward the background level. For this reason dates are not exact. Secondary peaks within 4 d of larger peaks are excluded from this list as they are considered to be the same event. In Table S2 we have also calculated accumulated cyclone energy (ACE) and US-ACE over the week centered on the date shown. We caution against comparing the relative rank of individual events. The surge index ranking reflects the impact at the specific tide-gauge locations and therefore should not be interpreted as a storm ranking. The purpose of this list is to demonstrate that the surge index truly captures cyclone activity, rather than providing a storm severity ranking.

A few events outside the hurricane season cannot be attributed to tropical cyclones. Several of these events, however, show up in other records of extreme weather; e.g., the large March 13, 1993 event is commonly known as the 1993 superstorm (1). NOAA has an extensive record of this event.

S3. GEV Distribution Fitting. The general method of fitting a distribution (f), with parameters (m), to a series (x) involves maximizing the likelihood function

$$L(m) = \prod_i f_m(x_i), \qquad \textbf{[S1]}$$

where i is an index into the series x. In practice, this is usually done by minimizing $-\log(L)$. The method can be easily extended to nonstationary distributions by having m vary with time (i). In this study, we achieve this by letting m be dependent on global temperature. The calculation of L can easily be parallelized and for some distribution functions it may be advantageous to perform this calculation on a graphical processing unit.

The confidence intervals of the model parameters are given by the likelihood function. We sample the parameter space according to the likelihood density, using Markov chain Monte Carlo (MCMC) using the Metropolis–Hastings algorithm (2). Regions of the parameter space that are likely will be sampled with a high density whereas less likely regions will be sampled less densely. From the percentiles of the sampling density we determine the confidence intervals. In this study we denote the median of the likelihood distribution as the "best guess" that is more robust than using the maximum-likelihood model.

We verify convergence of the MCMC solutions by manual inspection of the accepted models and their autocorrelation structure. In this study, our likelihood functions are very cheap to calculate, and we can afford to make the MCMC runs much longer than is strictly necessary. We speed up convergence, by taking random steps in a linearly transformed model space chosen on the basis of a principal component analysis (PCA) of the accepted models from an initial shorter MCMC run. We observe that the burn-in is usually confined to the shorter initial MCMC run, and that the transformed steps almost always gives near optimal rejection rates.

Under certain conditions the central limit theorem states that the sum of a set of independent random variables will approach a normal distribution in the limit of infinitely large sets. Analogously, the distribution of block maxima approaches the generalized extreme value (GEV) distribution as the blocks get larger (3). For that reason we expect that block maxima of the surge index should follow a GEV distribution. The GEV distribution, used in this study, can be described by

$$f_{m=(k,\mu,\sigma)}(x)=\begin{cases}\dfrac{1}{\sigma}\left(1+k\dfrac{x-\mu}{\sigma}\right)^{-1-\frac{1}{k}}e^{-\left(1+k\frac{x-\mu}{\sigma}\right)^{-\frac{1}{k}}} & \text{for } 1+\dfrac{k(x-\mu)}{\sigma}>0 \text{ and } k\neq 0\\ \dfrac{1}{\sigma}e^{\frac{\mu-x}{\sigma}-e^{\frac{\mu-x}{\sigma}}} & \text{for } k=0\\ 0 & \text{otherwise,}\end{cases}\qquad \textbf{[S2]}$$

where μ, σ, and k are the location, scale, and shape parameters, respectively. In the MCMC inference of the GEV model we use the conventional uniform priors on μ, log(σ), and k.

We are interested in the return period of large and rare events. We find that the surge index maxima of 7-d blocks can be accurately modeled by the GEV distribution over a wide range of magnitudes (Fig. 3). Sensitivity tests show that our results are not sensitive to larger block sizes. The GEV distribution is flexible and combines three simpler types of distributions commonly used to model block maxima: the Weibull, Frechet, and Gumbel distributions. The flexibility lets the data decide which distribution is appropriate.

It is sometimes argued (e.g., ref. 3) that taking block maxima is a wasteful method to infer statistics of extreme events. The reasoning is that there may be a small chance that two very large events are inside the same block and that taking block maxima could be discarding one of the already rare large events. The peaks-over-threshold (POT) method is the usual proposed alternative, where a distribution is fitted to all events that are above a certain threshold. The advantage is that no large events are discarded. The drawback of the POT approach is that return periods can be calculated only if the frequency of threshold crossing is known. The threshold return period can be estimated using empirical cumulative distribution. However, this empirical estimate assumes stationarity and the POT method is hence ill-suited for nonstationary series. For that reason we use exclusively the GEV distribution. However, our conclusions are insensitive to different block sizes and we get compatible results using POT analysis; we conclude that extreme event wastage is not an issue.

1. Kocin PJ, Schumacher PN, Morales RF, Uccellini LW (1995) Overview of the 12–14 March 1993 superstorm. *Bull Am Meteorol Soc* 76:165–182.
2. Hastings WK (1970) Monte Carlo sampling methods using Markov chains and their applications. *Biometrika* 57:97–109.
3. Coles S (2001) *An Introduction to Statistical Modeling of Extreme Values* (Springer, London).

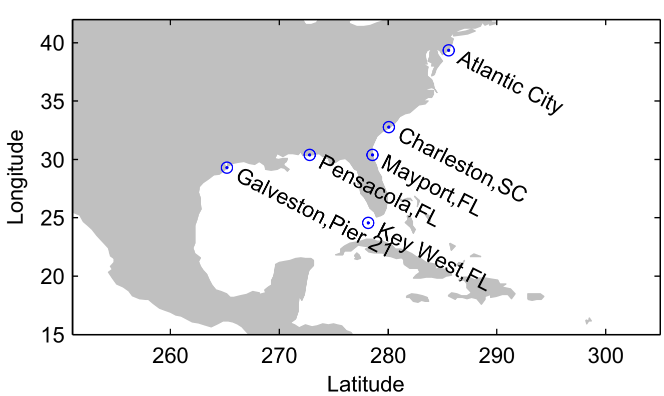

Fig. S1. Map showing locations of tide gauges used in the construction of the surge index.

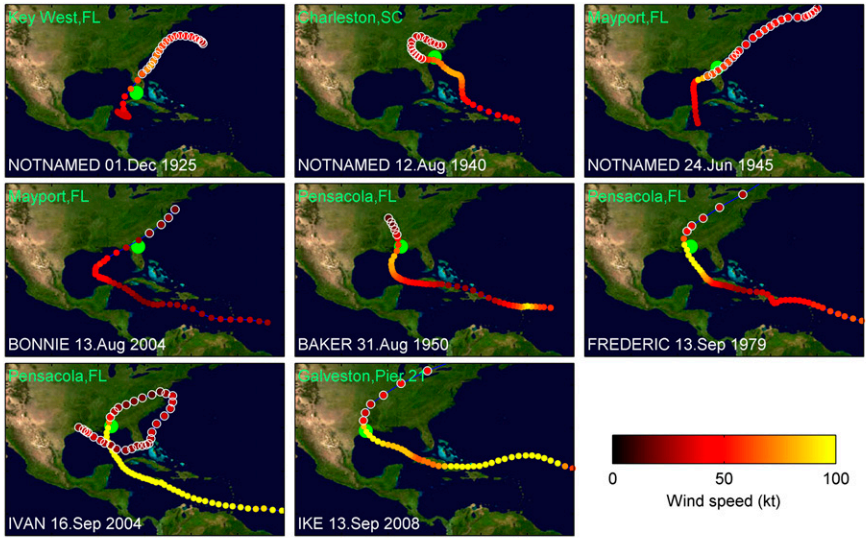

Fig. S2. Tracks of storms (blue line) that likely are the cause of gaps in the tide-gauge records. Red-yellow dots indicate wind speed at 6-h intervals; green shows tide-gauge location. White circles indicate when the tide gauge has missing data.

Table S1. Tide-gauge data gaps that coincide with storm landfall

Tide gauge	Gap start	Wind, kt	Distance, km	Storm name
Key West, FL	Dec. 1, 1925; 07:00	65	158	Not named
Charleston, SC	Aug. 12, 1940; 07:00	70	77	Not named
Mayport, FL	June 24, 1945; 03:00	95	118	Not named
Mayport, FL	Aug. 13, 2004; 06:00	45	128	Bonnie*
Pensacola, FL	Aug. 31, 1950; 14:00	83	63	Baker
Pensacola, FL	Sept. 13, 1979; 17:00	115	119	Frederic
Pensacola, FL	Sept. 16, 2004; 18:00	115	60	Ivan
Galveston, Pier 21	Sept. 13, 2008; 15:00	95	8	Ike

List of HURDAT storms that coincide with data gaps in the tide-gauge records (see text for selection criteria). "Gap start" shows the date of the first missing sample. "Wind" shows the maximum wind speed in the 24-h days preceding the gap. "Distance" refers to the closest distance to tide gauge in the 24 h centered on the gap start.
*Tropical storm Bonnie had similar timing to hurricane Charley and both could be responsible for the tide-gauge outage.

Table S2. 50 greatest events

Rank	Event date	Candidate storm (category)	Surge index	ACE	US-ACE	Wind, kt
1	Sept. 20, 1926	"Great Miami hurricane" (4)	283	422,098	228,174	125
2	July 25, 1934	Not named (1)	153	39,450	39,450	65
3	Sept. 19, 1947	Not named (5)	139	223,806	223,806	130
4	Sept. 10, 1961	Carla (5)	114	588,267	312,007	125
5	Aug. 30, 2005	Katrina (5)	113	189,274	167,424	110
6	July 10, 2005	Dennis (4)	107	207,799	188,024	120
7	Sept. 12, 2008	Ike (4)	104	146,499	143,599	100
8	Sept. 10, 1965	Betsy (4)	94	169,699	169,699	135
9	Sept. 1, 1932	Not named (1)	89	172,324	65,775	70
10	June 28, 1957	Audrey (4)	86	79,474	79,474	125
11	Sept. 27, 1998	Georges (4)	85	463,173	155,699	95
12	Sept. 1, 2008	Gustav (4)	70	326,423	300,849	125
13	Oct. 6, 1995	Opal (4)	59	180,099	91,975	110
14	Aug. 5, 1940	Not named (1)	57	117,449	117,449	70
15	Aug. 18, 1969	Camille (5)	57	362,419	217,996	165
16	Aug. 13, 1932	Not named (4)	55	64,600	64,600	125
17	Oct. 25, 2005	Wilma (5)	55	190,674	161,224	110
18	July 15, 2003	Claudette (1)	55	81,050	56,875	75
19	Oct. 4, 1964	Hilda (4)	53	166,994	166,994	83
20	Sept. 15, 2004	Ivan (5)	53	406,723	364,298	105
21	Aug. 17, 1983	Alicia (3)	52	68,500	68,500	100
22	Aug. 31, 1942	Not named (3)	49	162,324	93,275	70
23	Aug. 26, 1926	Not named (3)	48	110,974	110,974	95
24	Sept. 27, 2002	Isidore (3)	47	180,174	180,174	110
25	8-Sep-1974	Carmen (4)	47	168,899	124,474	120
26	Sept. 12, 1979	Frederic (4)	42	272,524	134,274	115
27	Sept. 25, 1941	Not named (1)	40	229,774	57,725	70
28	April 8, 1938		39			
29	Sept. 19, 1928	Not named (5)	39	152,974	152,974	140
30	Feb. 27, 1984		39			
31	Sept. 30, 1959	Gracie (4)	36	281,526	104,798	96
32	Aug. 9, 1980	Allen (5)	36	345,148	345,148	100
33	Sept. 24, 2005	Rita (5)	35	253,274	222,699	100
34	March 14, 1993		35			
35	Sept. 11, 1964	Dora (3)	35	307,606	121,637	83
36	Oct. 28, 1985	Juan (1)	34	79,850	79,850	65
37	June 12, 2005	Arlene (0)	34	31,175	31,175	50
38	Feb. 25, 1965		33			
39	Sept. 2, 1985	Elena (3)	33	145,274	145,274	100
40	Aug. 3, 1933	Not named (1)	31	63,500	63,500	70
41	July 6, 1933	Not named (2)	31	118,524		70
42	July 30, 1995	Erin (1)	30	65,150	65,150	80
43	Sept. 5, 1979	David (5)	29	206,774	158,549	150
44	Sept. 22, 1948	Not named (3)	29	143,824	143,824	90
45	Oct. 19, 1944	Not named (3)	29	124,557	124,557	58
46	Oct. 5, 1949	Not named (3)	28	75,853	75,853	112
47	Dec. 7, 1969		28			
48	July 24, 1933	Not named (0)	27	69,000	69,000	40
49	Aug. 4, 1995	Erin (1)	26	68,925	68,925	80
50	Jan. 21, 1979		26			

ACE and US-ACE are calculated over the week centered at the date shown. Wind shows the maximum landfalling wind speed.